Cell, Vol. 103, 99–111, September 29, 2000, Copyright ©2000 by Cell Press

ICEBERG: A Novel Inhibitor of Interleukin-1β Generation

Eric W. Humke,*† Stephanie K. Shriver,‡ Melissa A. Starovasnik,‡ Wayne J. Fairbrother,‡§ and Vishva M. Dixit†§

*Department of Cellular and Molecular Biology
University of Michigan Medical School
Ann Arbor, Michigan 48109
†Department of Molecular Oncology
‡Department of Protein Engineering
Genentech, Inc.
South San Francisco, California 94080

Summary

ProIL-1β is a proinflammatory cytokine that is proteolytically processed to its active form by caspase-1. Upon receipt of a proinflammatory stimulus, an upstream adaptor, RIP2, binds and oligomerizes caspase-1 zymogen, promoting its autoactivation. ICEBERG is a novel protein that inhibits generation of IL-1β by interacting with caspase-1 and preventing its association with RIP2. ICEBERG is induced by proinflammatory stimuli, suggesting that it may be part of a negative feedback loop. Consistent with this, enforced retroviral expression of ICEBERG inhibits lipopolysaccharide-induced IL-1β generation. The structure of ICEBERG reveals it to be a member of the death-domain-fold superfamily. The distribution of surface charge is complementary to the homologous prodomain of caspase-1, suggesting that charge–charge interactions mediate binding of ICEBERG to the prodomain of caspase-1.

Introduction

Members of the caspase family of aspartate-specific cysteine proteases play a crucial role in both apoptosis and inflammation. The first mammalian member of this family cloned, interleukin-1β converting enzyme (ICE), now termed caspase-1 (for *c*ysteinyl *asp*artate-specific prote*ase*), was originally discovered as the cytoplasmic protease responsible for the conversion of the 34 kDa inactive precursor IL-1β to the mature 17 kDa proinflammatory cytokine (Cerretti et al., 1992; Thornberry et al., 1992; Miller et al. 1993). Caspase-1 has since been shown to process the cytokine precursor of IL-18 (interferon-γ-inducing factor) (Ghayur et al., 1997; Gu et al., 1997). Underscoring the importance of this protease in cytokine processing is the finding that caspase-1-deficient mice are remarkably resistant to LPS-induced endotoxic shock. Thus, caspase-1 is an attractive target for therapeutic intervention in inflammatory diseases (Kuida et al., 1995; Li et al., 1995).

Caspase-1 is synthesized as a single-chain polypeptide zymogen consisting of an N-terminal prodomain, and a large (p20) and a small (p10) catalytic domain (Thornberry et al., 1992). The zymogen has low but detectable enzymatic activity. Upon receipt of a proinflammatory signal, caspase-1 is thought to oligomerize and autoprocess to generate the active p10/p20 heterodimeric protease (Walker et al., 1994; Wilson et al., 1994; Ghayur et al., 1997). The N-terminal prodomain appears to play a critical role in this oligomerization-based activation of caspase-1 since its removal prevents processing (Van Criekinge et al., 1996).

At least one potential mechanism by which caspase-1 is regulated became evident with the identification of a serine/threonine kinase RIP2/CARDIAK/RICK (Inohara et al., 1998; McCarthy et al., 1998; Thome et al., 1998) that binds caspase-1 and promotes its processing (Thome et al., 1998). RIP2 engages caspase-1 through a direct protein–protein interaction involving corresponding caspase recruitment domains (CARDs) present at the C terminus of RIP2 and within the prodomain of caspase-1 (Hofmann et al., 1997; Thome et al., 1998). The CARD module mediates the interaction between a number of large prodomain caspases and their corresponding upstream activator adaptors, the prototypical examples being caspase-9 and Apaf-1 (Zou et al., 1997, 1999; Day et al., 1999; Qin et al., 1999). Structurally, the CARD motif resembles the death domain (DD) and the death effector domain (DED). All possess six helices and have a propensity to self associate. These homotypic interaction motifs form the molecular glue that bind the signaling machinery responsible for caspase activation (for a review, see Hofmann, 1999).

One powerful way to modulate assembly of such signaling complexes is through the presence of "decoy" molecules that attenuate the assembly process. The most dramatic examples of this are virally encoded DEDs from a number of γ-herpesviruses including two human oncogenic viruses (Kaposi sarcoma associated-herpesvirus and molluscum contagiosum virus) that bind the DEDs of FADD and/or caspase-8 (FLICE) and disrupt assembly of the Fas-receptor associated death inducing signaling complex (Hu et al., 1997; Thome et al., 1997). These viral proteins, termed v-FLIPs (for *v*iral *FL*ICE *i*nhibitory *p*roteins), function to effectively switch off proapoptotic signaling from the Fas death receptor (for reviews see Tschopp et al., 1998a, 1998b). The v-FLIPs are closely related to c-FLIP, an endogenous cellular protein present as various splice forms, the longest of which (c-FLIP$_L$) is a potent inhibitor of FADD-mediated caspase-8 activation (Hu et al., 1997; Irmler et al., 1997). Therefore, both viral and cellular decoy molecules are capable of regulating assembly of signaling complexes held together by homotypic interactions involving six-helix-bundle interaction domains. In a similar vein, we find that activation of caspase-1 and subsequent generation of IL-1β is regulated by a small CARD-containing decoy molecule termed ICEBERG. This decoy protein binds the corresponding CARD motif present in the prodomain of caspase-1, inhibiting and/or displacing the upstream activator RIP2. ICEBERG works through this mechanism to attenuate inflammation. The induction of ICEBERG by proinflammatory stimuli is con-

§To whom correspondence should be addressed (e-mail: fairbro@gene.com [W. J. F.], dixit@gene.com [V. M. D.])

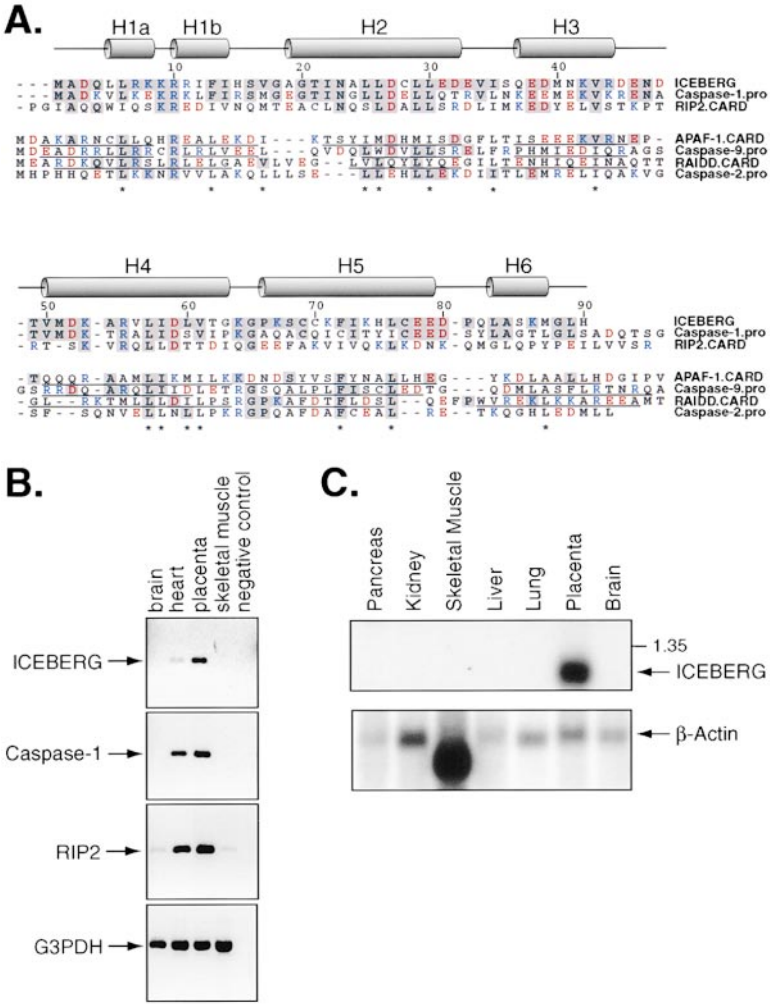

Figure 1. Sequence and Expression of ICEBERG

(A) Structural alignment of full length ICEBERG with other CARD domains using the single letter amino acid code. The locations of the helices within ICEBERG are represented as cylinders above the alignment. Helical regions of other CARDs whose structures have been solved are underlined. The charged residues are colored (blue = basic, red = acidic). Starred residues are hydrophobic and packed at the core of ICEBERG. Shading denotes residues identical to ICEBERG.

(B) Expression of ICEBERG. Human adult cDNA panels were amplified with primers specific for either ICEBERG, RIP2, caspase-1, or glyceraldehyde-3 phosphate dehydrogenase (G3PDH). Tissues not shown include kidney, lung, liver, and pancreas.

(C) Human adult tissue Northern blot probed with ICEBERG cDNA.

sistent with it being a novel negative-feedback loop that serves to eventually shut off IL-1β generation.

Results

Identification of ICEBERG

The public EST database was searched for sequences with significant homology to the CARD-containing prodomain of caspase-1 to identify regulators of caspase-1 activation. A novel 500 bp cDNA clone was identified that encoded an open reading frame with a predicted molecular mass of 10.1 kDa. This protein, termed ICEBERG, is 52% identical to the caspase-1 CARD (Figure 1A). Analysis of multiple tissue cDNA panels and northern blots revealed that ICEBERG is primarily expressed in the heart and placenta (Figures 1B and 1C). The related CARD-containing molecules caspase-1 and RIP2 are also expressed in the heart and placenta as well as in numerous other tissues (Figure 1B).

ICEBERG Binds Caspase-1

Based on sequence homology and the homotypic nature of six-helix-bundle, death-domain-fold superfamily members, we reasoned that ICEBERG would likely bind caspase-1 through the cognate CARD-containing segments (Figure 2A, left panels). In keeping with this notion, removal of caspase-1 prodomain was found to abolish its binding to ICEBERG (Figure 2A, right panels). Using bacterially expressed and purified ICEBERG and caspase-1 prodomain, coimmunoprecipitation of the prodomain of caspase-1 is sufficient for direct ICEBERG interaction (Figure 2B). To ensure binding was not due to promiscuous CARD–CARD interactions, ICEBERG was incubated with other CARD-containing molecules; it did not bind caspase-7, caspase-8, caspase-9, or RIP2 (Figure 2C and data not shown).

RIP2 Activates Caspase-1

The concept that oligomerization promotes autoprocessing was originally proposed in studies where overexpressed zymogen was found to process itself to active protease (Gu et al., 1995). Further studies suggested that zymogen self-association occurs through the prodomain (Van Criekinge et al., 1996). Consistent with this idea, replacing the prodomain with an artificial oligomerizer will promote activation (MacCorkle et al., 1998; Muzio et al., 1998a; Srinivasula et al., 1998; Yang et al., 1998). Activation of many large prodomain regulatory caspases, including caspase-9, CED-3, and caspase-8, results from induced proximity mediated by association

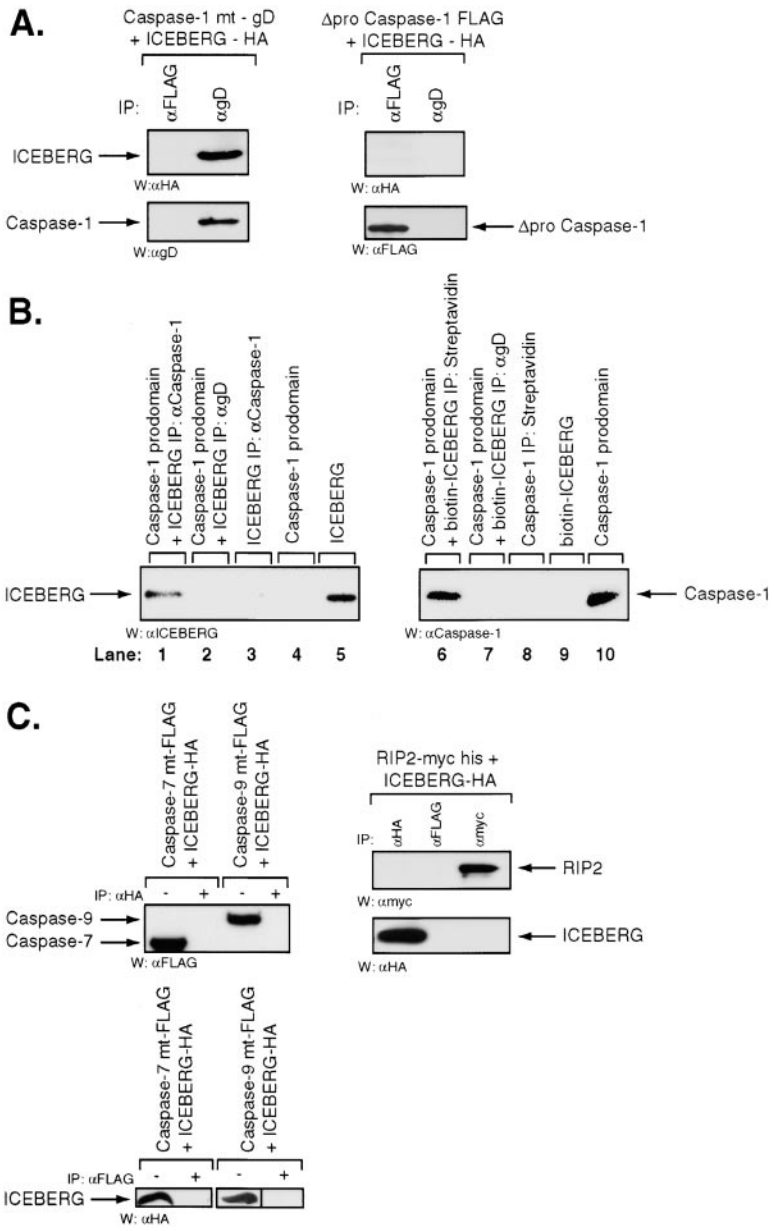

Figure 2. Characterization of ICEBERG/Caspase-1 Binding

(A) Interaction of ICEBERG with full length caspase-1 (left panels). Removal of the caspase-1 prodomain results in loss of ICEBERG binding (right panels). Abbreviations for constructs include caspase-1 catalytic cysteine to alanine mutant (abbreviated mt) and caspase-1 with no prodomain (Δpro).

(B) Interaction of purified ICEBERG and purified prodomain of caspase-1. ICEBERG immunoprecipitates with caspase-1 (left panel, lane 1) and caspase-1 immunoprecipitates with ICEBERG (right panel, lane 6). Monoclonal gD antibody was used for the control immunoprecipitation (lanes 2 and 7). Lanes 3, 4, 8, and 9 are negative controls. Lanes 5 and 10 are positive controls.

(C) ICEBERG does not interact with RIP2 or other CARD-containing molecules including caspase-9 and caspase-7. 293T cells were transfected with the indicated plasmids and immunoblotted as in (A).

with their respective upstream adaptor molecules APAF-1, CED-4, and FADD. The adaptor molecules function to concentrate caspase zymogens so that neighboring molecules accurately process each other at internal Asp residues to generate the two-chain active enzyme (for a review, see Salvesen and Dixit, 1999).

RIP2/CARDIAK has been shown to bind and activate caspase-1 (Thome et al., 1998). The ability of RIP2 and caspase-1 to physically interact was further characterized to investigate if RIP2 mediated oligomerization of caspase-1 promoted its activation. 293T cells were transiently cotransfected with RIP2 myc-his and caspase-1 gD followed by immunoprecipitation with either RIP2 or gD antibody. RIP2 bound caspase-1 quantitatively; the converse was also true (Figure 3A). To determine if the interaction was through the CARD motif, RIP2-CARD was expressed as a fusion to glutathione-S-transferase (GST) and immobilized onto glutathione-Sepharose. The RIP2-CARD bound purified caspase-1 prodomain, confirming that the purified CARDs could directly bind (Figure 4D, lane 2). The self-association of the zymogen form of caspase-1 upon overexpression was demonstrated using differentially epitope-tagged forms of the molecule (Figure 3B, lane 1). However, in the presence of RIP2, caspase-1 self-association was enhanced and autoactivation evident as judged by generation of processed subunits (Figure 3B, lane 2; Figure 3C). This was further demonstrated using purified components (Figure 4E, lane 3). Therefore, RIP2 enhances the activation of caspase-1 by promoting its oligomerization in accord with the induced proximity model.

ICEBERG Inhibits the Ability of RIP2 to Oligomerize Caspase-1

Given that oligomerization of caspase-1 initiates its activation, this step is likely to be highly regulated. To deter-

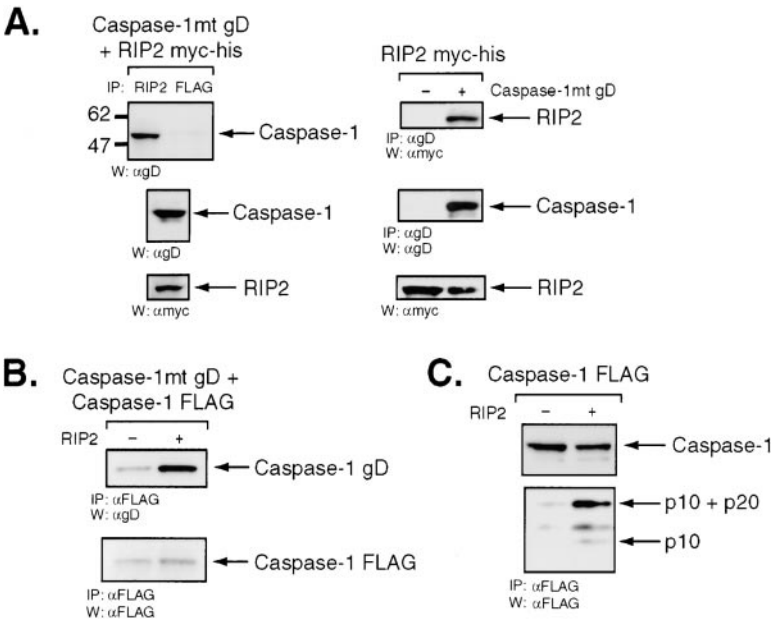

Figure 3. RIP2 Oligomerization and Activation of Caspase-1

(A) RIP2 binds caspase-1 (left and right upper panels). Lower four panels show expression of RIP2 and caspase-1 in the lysate used for immunoprecipitation.

(B) RIP2 oligomerizes caspase-1. Differentially tagged versions of caspase-1 were cotransfected in the presence (right lane) or absence (left lane) of RIP2, immunoprecipitated with FLAG-M2 beads (Sigma) and probed with gD antibody to look for self-association between differentially tagged caspase-1 proteins. The blot was reprobed with αFLAG to normalize for caspase-1 expression.

(C) RIP2 activates caspase-1. Caspase-1 was expressed in the presence (right lane) or absence of RIP2 (left lane). Lysate was immunoprecipitated with αFLAG and Western blotted with αFLAG.

mine if ICEBERG inhibits the ability of RIP2 to oligomerize caspase-1, 293T cells were transiently transfected with RIP2 V5, caspase-1 gD, and caspase-1 FLAG with or without ICEBERG HA. As noted previously, overexpressed caspase-1 oligomerized and this was enhanced by RIP2 expression (Figures 3B and 4A, lane 1 versus lane 3). However, in the presence of ICEBERG, RIP2-mediated enhancement of oligomerization was inhibited (Figure 4A, lane 5 versus lane 7). Consistent with this result, caspase-1 was no longer complexed to RIP2 but now bound ICEBERG (Figure 4B, right panels). The ability of ICEBERG to act as a potential regulator of caspase-1 activation was reaffirmed by showing ICEBERG inhibits RIP2 mediated processing of caspase-1 (Figure 4C). Using purified recombinant proteins, we assessed if the binding and inhibition by ICEBERG was direct. RIP2-CARD expressed as a GST-fusion was immobilized onto glutathione beads and incubated with soluble caspase-1; ICEBERG was then added at an equimolar ratio for defined time periods. The RIP2/caspase-1 complex was disrupted by the added ICEBERG as ICEBERG preferentially bound caspase-1, leading to the release of caspase-1 from the RIP2 beads (Figure 4D, upper panel). This was confirmed by immunoprecipitating displaced caspase-1 from the soluble fraction and finding it in complex with ICEBERG (Figure 4D, lower panel). The possibility that ICEBERG was disrupting the RIP2/caspase-1 complex by binding RIP2 was discounted because ICEBERG did not bind RIP2-CARD GST (data not shown) or full length RIP2 (Figure 2C). The ability of RIP2 to activate purified caspase-1 was inhibited by purified ICEBERG (Figure 4E, lane 4). Therefore, ICEBERG, by preferentially binding caspase-1, inhibits RIP2-mediated oligomerization of caspase-1 and, presumably, the subsequent generation of downstream active caspase-1 and IL-1β.

ICEBERG Is Upregulated by LPS and TNF and Inhibits IL-1β Release from Monocytes

THP.1 monocytes release IL-1β in response to an inflammatory stimulus such as LPS. To test whether ICEBERG could inhibit IL-1β generation, it was expressed in these cells under the control of a retroviral promoter. The generation of IL-1β upon LPS stimulation was significantly blunted in ICEBERG-expressing cells, consistent with the biochemical studies (Figure 5).

While the exact details of how caspase-1 is activated following LPS stimulation remain unclear, what is apparent is that cytokine generation and inflammation must eventually be turned off. We hypothesized that ICEBERG may fulfill such a role by acting as a physiologic inhibitor of IL-1β generation. The production of IL-1β by immune cells upon an inflammatory stimulus is a rapid posttranslational event, with active cytokine generated in minutes. It would make teleological sense for inhibitors of the system to be dependent upon relatively slow new gene transcription/translation so that in the hours it takes to generate them, the beneficial effects of inflammation have begun to take place. Given this, we asked if ICEBERG transcript was inducible by proinflammatory agents such as LPS or TNF. Using exon-specific primers and RT-PCR, ICEBERG transcript was found to be LPS- and TNF-inducible (Figure 6A). This is a general phenomenon confined not only to THP.1 cells, but also observed with primary monocytes and endothelial cells (Figure 6A, lower six panels). Additionally, metabolic labeling and immunoprecipitation revealed ICEBERG protein was also induced by LPS, being detectable 7 hr poststimulation (Figure 6B, lower panels). This induction of ICEBERG coincided with reduction in caspase-1 activity (Figure 6B, lower graphs) and corresponding reduction in IL-1β release (Figure 6B, upper graphs). Therefore, after exposure to LPS, there occurs an initial rapid burst of caspase-1 activation and IL-1β release, both of which are rapidly attenuated coincident with the appearance of ICEBERG protein. This is in keeping with the proposed negative feedback role of ICEBERG in regulating IL-1β production.

Endogenous Modulation of Caspase-1 in Response to LPS

We generated monoclonal antibodies specific for RIP2 and caspase-1 to investigate the interactions observed

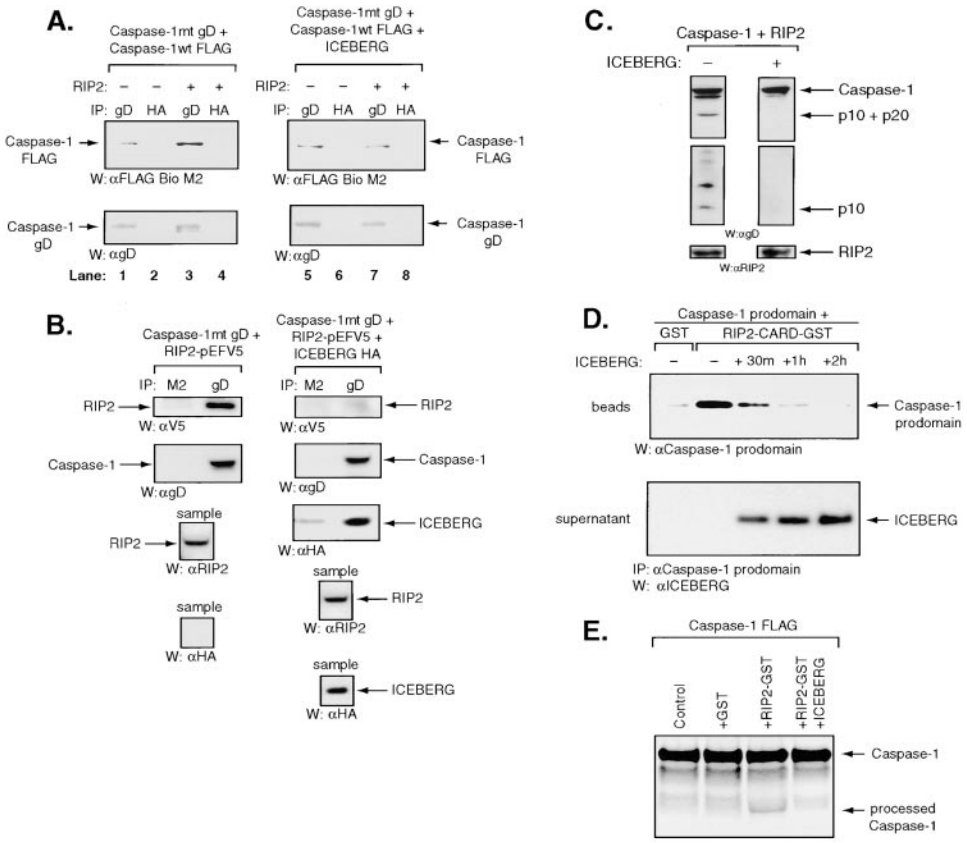

Figure 4. ICEBERG Inhibits RIP2 Oligomerization and Activation of Caspase-1

(A) Caspase-1 oligomerization enhanced in the presence of RIP2 (lane 3 versus lane 1) is inhibited in the presence of ICEBERG (lane 7 versus 5). Negative control HA antibody is shown in lanes 2, 4, 6, and 8. Stable cells with or without ICEBERG were transfected with plasmids expressing differentially tagged caspase-1 (as in Figure 3B). The coprecipitating caspase-1 was detected using a biotinylated αFLAG antibody (Sigma) and visualized with streptavidin-peroxidase (Sigma; upper panel).

(B) RIP2 does not bind caspase-1 in the presence of ICEBERG as caspase-1 is bound to ICEBERG (upper right panels, right lane). RIP2 binds caspase-1 in the absence of ICEBERG (upper left panel, right lane).

(C) The ability of RIP2 to activate caspase-1 is inhibited by ICEBERG. Stable cells with or without ICEBERG were cotransfected with RIP2 and caspase-1-gD. The clarified lysate was Western blotted with a gD antibody. RIP2 protein in the lysate is shown in the lower two panels.

(D) Purified ICEBERG displaces caspase-1 from RIP2. Caspase-1 prodomain was incubated with glutathione beads containing either RIP2-CARD-GST or GST alone. After incubation, ICEBERG was added at an equimolar ratio to caspase-1. Washed beads were blotted for the presence of caspase-1 prodomain (upper panel). The washes were precipitated for caspase-1 prodomain and Western blotted for the presence of ICEBERG (lower panel).

(E) ICEBERG inhibits the ability of RIP2 to activate caspase-1 in a purified system. In vitro translated caspase-1 was incubated in activation buffer containing either RIP2-CARD-GST or GST bound to glutathione beads in the presence or absence of ICEBERG.

with transfected molecules at the endogenous level. By immunoprecipitation and subsequent immunoblotting, we found that RIP2, as expected, associated with caspase-1 in an LPS dependent manner (Figure 7A). The converse was also true (Figure 7B). The likely transient nature of the activation complex between endogenous RIP2 and caspase-1 is reflected in the fact that upon LPS activation, only a small fraction of total caspase-1 is found associated with RIP2 (compare lane 1 and 4, Figure 7B). Indeed, this transient association made detection problematic, requiring the use of large numbers of cells and metabolic labeling to high specific activity. Under these conditions, a weak association was observed between endogenous RIP2 and caspase-1 that was significantly enhanced upon LPS activation (compare lanes 3 and 4, Figure 7B). To detect endogenous ICEBERG complexed to caspase-1, metabolically labeled THP.1 cells were pretreated for 12 hr with LPS (to induce ICEBERG), followed by immunoprecipitation analysis. As shown (Figure 7C), caspase-1 antibody (lane 3) but not control antibody (lane 2) coprecipitated ICEBERG.

ICEBERG Solution Structure

Since modulators of caspase-1 activation represent attractive therapeutic targets, we determined the structure of ICEBERG as a first step toward understanding the molecular basis of its interaction with caspase-1. The solution structure of ICEBERG was determined using data from 3D heteronuclear NMR spectra obtained using uniformly ^{15}N-labeled and $^{15}N/^{13}C$-labeled protein samples at pH 3.8 (at pH values $\geq$ 4.3, ICEBERG forms a gel at concentrations required for NMR structure determination). The final structure is based on a total of 1238 experimentally derived internuclear distance and dihedral angle restraints. The structure of ICEBERG is well

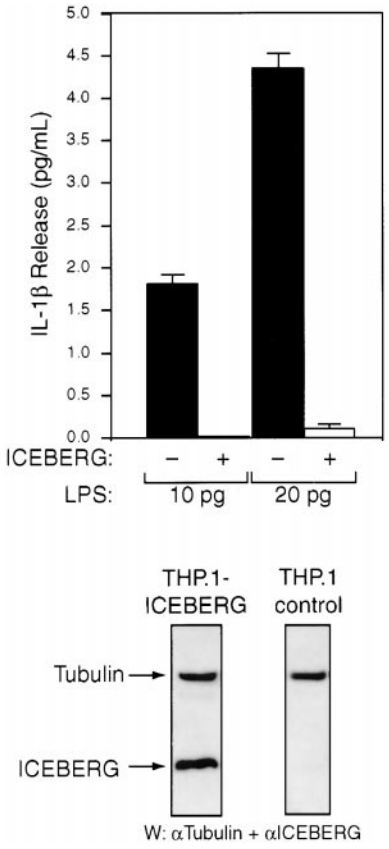

Figure 5. ICEBERG Inhibits LPS Inducible IL-1β Production

ICEBERG was expressed in THP.1 cells following infection with an engineered retrovirus (Hawley et al., 1996). After LPS stimulation for 6 hr, total IL-1β release from clonal cells was quantitated using an IL-1β ELISA. Graph shows representative data from four independent experiments. ICEBERG expression is shown relative to tubulin (lower panels).

defined by the data (Table 1); the covalent geometry is also good with 84% of the ϕ,ψ angles within the most favored regions of a Ramachandran plot for residues 5–89. The protein forms an antiparallel six-helix bundle with Greek-key topology and a well-defined hydrophobic core (Figure 8). Helices H1–H5 are α-helical while H6 is a 3_{10} helix; H1 is interrupted by a distinct kink at residue Lys9. As expected based on sequence comparisons (Figure 1A), the global fold of ICEBERG places it in the death-domain structural superfamily that includes DDs (Huang et al., 1996; Liepinsh et al., 1997; Jeong et al., 1999), DEDs (Eberstadt et al., 1998), and CARDs (Chou et al., 1998; Day et al., 1999; Qin et al., 1999; Vaughn et al., 1999; Zhou et al., 1999).

The structure of ICEBERG is most similar to those determined recently for the CARDs of RAIDD (Chou et al., 1998), Apaf-1 (Qin et al., 1999; Vaughn et al., 1999; Zhou et al., 1999), and the prodomain of caspase-9 (Qin et al., 1999). The best-fit superpositions of Cα atoms yielded RMSDs of 1.6 Å for 77 pairs of residues, 1.9 Å for 81 pairs of residues, and 2.0 Å for 76 pairs of residues for Apaf-1, caspase-9, and RAIDD CARDs, respectively. Structural alignment of the four CARDs reveals a number of conserved hydrophobic residues that make up the core of the domains (Figure 1A). There are several differences, however, in the packing of the cores, as well as in the loops between the helices and the lengths of the helices; in particular, helices H1 and H6 are significantly shorter in ICEBERG than in the other CARD structures.

The surface of ICEBERG contains three highly charged patches (Figure 9A). Five basic residues from helix H1 (Arg7, Lys8, Lys9, Arg10, and Arg11), together with Arg55 from H4 and Lys86 from H6, form a positively charged patch on one surface. The opposite surface is predominantly negatively charged with acidic side chains contributed from the C-terminal ends of helices H2 (Asp27, Glu31, and Asp32) and H5 (Glu78 and Glu79); residues Glu33 and Asp80 might also be considered as part of this patch. A second negatively charged surface is found on the bottom of the structure, as presented in Figure 9A, comprising acidic residues from the H4–H5 turn (Asp45, Glu46, and Asp48) and Asp52 from H5.

A homology model of the prodomain of caspase-1 revealed a distribution of surface charge similar to ICEBERG, with a positively charged patch formed by residues from helices H1 and H4, and a negatively charged patch on the opposite surface formed by residues from helices H2 and H5 (Figure 9B). Similar to the RAIDD/caspase-2 and Apaf-1/caspase-9 interactions (Chou et al., 1998; Day et al., 1999; Qin et al., 1999; Vaughn et al., 1999; Zhou et al., 1999), we propose that charge–charge interactions are important for mediating the interaction between ICEBERG and caspase-1. Consistent with this suggestion, we observed no interaction between ICEBERG and the caspase-1 prodomain at pH 3.8, where the acidic patches on both proteins are likely protonated (data not shown).

The general similarity between the surface properties of ICEBERG and the caspase-1 prodomain raised questions regarding the binding specificity of RIP2 CARD, which binds to caspase-1 prodomain but not to ICEBERG (Figure 2C and data not shown). To gain some insight into these interactions we also built a homology model of RIP2 CARD (Figure 9C). RIP2 CARD has a dramatically different surface charge distribution relative to ICEBERG and caspase-1 prodomain. The positively charged patch centered around helix H1 in both ICEBERG and caspase-1 prodomain has been neutralized in RIP2 CARD, and, in addition, this face has a concave, negatively charged patch comprising residues from helix H3, the C-terminal region of H4, and the N-terminal region of H5. Furthermore, the opposite surface of RIP2 CARD does not possess a negatively charged patch as observed for ICEBERG and caspase-1 prodomain.

Discussion

ICEBERG was identified as a novel protein bearing high homology to the CARD of caspase-1. In vitro and in vivo binding data showed that ICEBERG specifically associates with the prodomain of caspase-1 and that this interaction inhibits binding of the upstream activator RIP2 to caspase-1. RIP2 has been shown previously to bind and activate caspase-1 (Thome et al., 1998). Our studies confirm and extend these observations by suggesting that RIP2 acts as a nidus for oligomerization of caspase-1

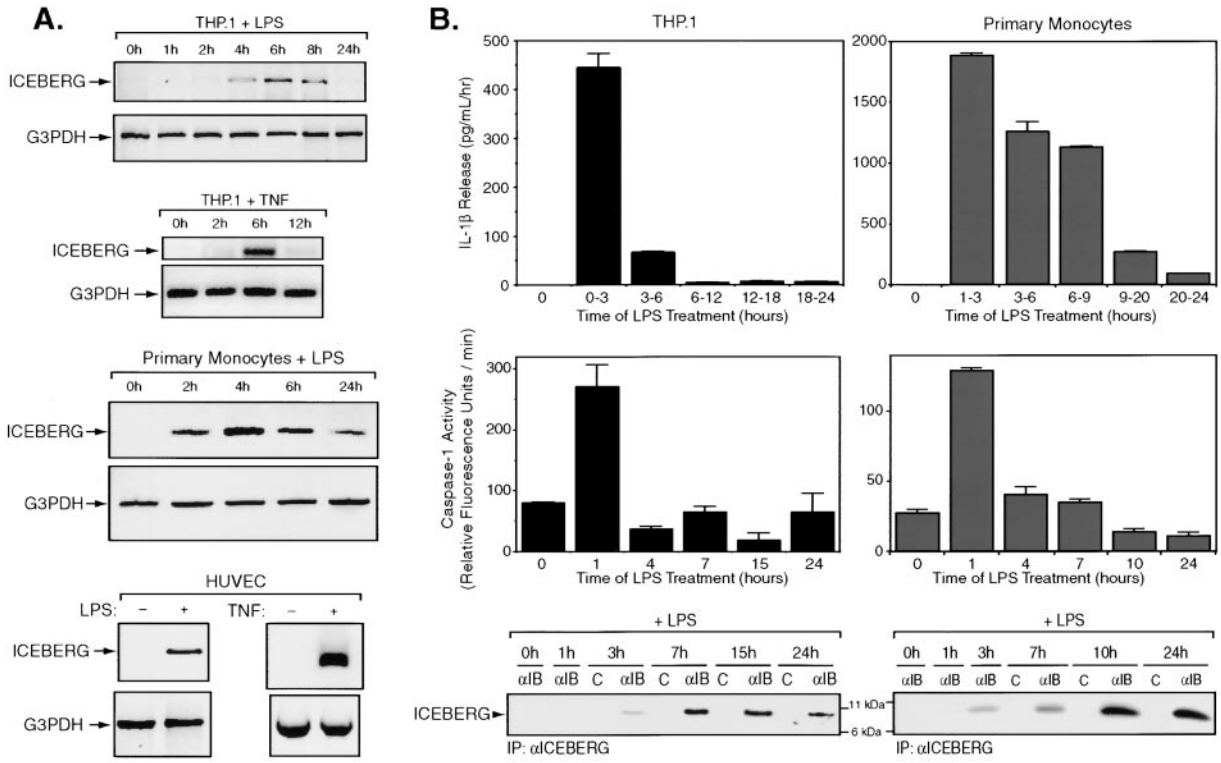

Figure 6. Lipopolysaccharide and Tumor Necrosis Factor Upregulate ICEBERG Expression

(A) Transcription of ICEBERG mRNA increases following LPS or TNF treatment. The amount of RNA was normalized using glyceraldehyde-3-phosphate specific primers (lower panel).

(B) ICEBERG protein is LPS inducible coincident with a decrease in IL-1β release and caspase-1 activity. THP.1 cells and primary monocytes were treated with LPS and supernatants assayed for IL-1β (upper bar graphs). Lysates prepared from LPS-treated THP.1 cells and primary monocytes were measured for their caspase-1 activity (middle bar graphs). To visualize ICEBERG, THP.1 cells and primary monocytes were treated with LPS, metabolically labeled, and immunoprecipitated (lower panels).

zymogen, thereby promoting its proteolytic autoactivation, keeping with the induced proximity model (Figures 3B and 3C). The association of RIP2 with caspase-1 is a rapid and transient posttranslational event captured only with difficulty at the endogenous level (Figures 7A and 7B). In contrast, ICEBERG is induced through new gene transcription and translation, a process that takes several hours (Figures 6A and 6B). Once present, however, it functions to inhibit the association of RIP2 with caspase-1 (Figure 4B) and will, in fact, even dissociate

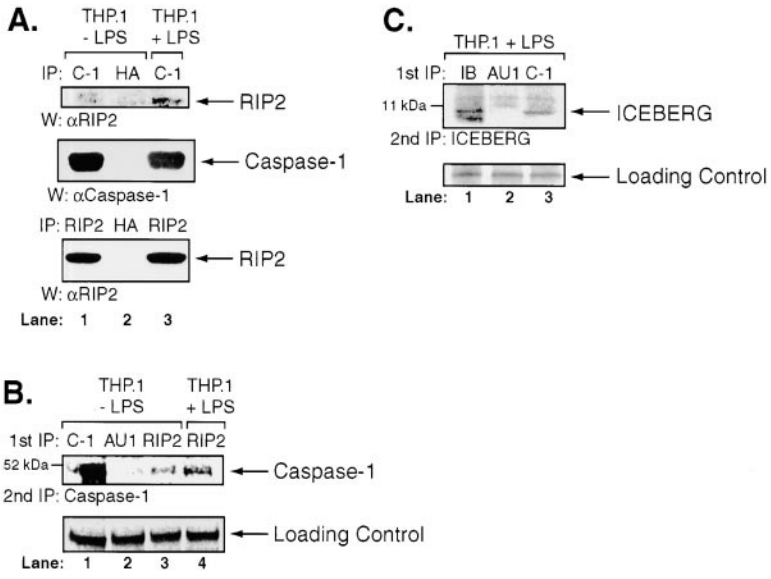

Figure 7. Endogenous Binding

(A) RIP2 binds caspase-1 in an LPS-dependent manner (upper panel, lane 3 versus lane 1). THP.1 cells were immunoprecipitated for caspase-1 and probed for RIP2. The amount of caspase-1 and RIP2 immunoprecipitated is shown in the lower panels.

(B) Caspase-1 binds RIP2 in an LPS-dependent manner (upper panel, lane 3 versus lane 4). Same as in Figure 7A; however, the THP.1 cells were metabolically labeled and immunoprecipitated for RIP2 followed by caspase-1.

(C) ICEBERG associates with caspase-1 in an LPS-dependent manner (upper panel, lane 3). Metabolically labeled THP.1 cells were immunoprecipited for caspase-1 followed by ICEBERG.

Table 1. Summary of Structural Statistics for the 20 Final Structures of ICEBERG

RMS deviation from experimental distance restraints (Å)	
NOE	
All (1050)	0.0084 ± 0.0006
Intraresidue (299)	0.0037 ± 0.0009
Sequential (264)	0.0115 ± 0.0017
Medium (249)	0.0090 ± 0.0011
Long ($\|i - j\| > 4$) (238)	0.0082 ± 0.0012
H-bonds (88)	0.0118 ± 0.0016
RMS deviation from experimental dihedral restraints (°)	
ϕ (84), χ^1 (16)	0.098 ± 0.050
NOE distance restraint violations	
No. violations > 0.1 Å	0.15 ± 0.37
Maximum violation (Å)	0.09 ± 0.01
Dihedral angle restraint violations	
No. violations > 1°	0.45 ± 0.51
Maximum violation (°)	0.96 ± 0.49
RMS deviations from idealized covalent geometry	
Bonds (Å) (1439)	0.0030 ± 0.0002
Angles (°) (2622)	0.372 ± 0.009
Planes (°) (696)	0.171 ± 0.006
Energies (kcal·mol^{-1})	
E_{NOE}[a]	4.37 ± 0.62
E_{CDIH}	0.07 ± 0.07
E_{bond}	12.9 ± 1.8
E_{angle}	55.4 ± 2.7
E_{plane}	3.1 ± 0.2
E_{vdW}[b]	10.6 ± 1.3
E_{total}	86.5 ± 5.6

[a] The final value of the square-well NOE (E_{NOE}) and torsion angle (E_{CDIH}) potentials are calculated with force constants of 50 kcal·mol^{-1}·Å^{-2} and 200 kcal·mol^{-1}·rad^{-2}, respectively.

[b] The quadratic van der Waals repulsion term (E_{vdW}) is calculated with a force constant of 4 kcal·mol^{-1}·Å^{-4} with the van der Waals radii set to 0.8 times the values in the XPLOR parameter set PARMALLH6 (Linge and Nilges, 1999).

preformed complexes of RIP2 and caspase-1 (Figure 4D). The net effect of its presence is to attenuate caspase-1 activation (Figures 4C and 4E and Figure 6B, lower graph) and IL-1β generation (Figure 6B, upper graph), a conclusion underscored by the finding that enforced retroviral expression of ICEBERG in THP.1 cells inhibits IL-1β generation in response to LPS (Figure 5).

The biological effects of IL-1β depend on where and how much of the cytokine is produced. At low concentrations, it functions primarily to mediate local inflammation, for example by causing mononuclear phagocytes and endothelial cells to synthesize chemokines that recruit and activate various leukocyte populations. However, if synthesized in larger quantities, it can exert potentially lethal systemic effects including fever, chills and shock (for reviews see Dinarello, 1997; O'Reilly et al., 1999). Therefore, it is important to keep IL-1β levels in check to prevent a fatal outcome on exposure to a minor proinflammatory insult. Reinforcing this notion is the fact that IL-1 is the only cytokine to date for which naturally occurring inhibitors have been described. IL-1 receptor antagonist (IL-1ra) is structurally related to IL-1 and binds IL-1 receptors but is biologically inactive, therefore functioning as a competitive inhibitor of IL-1 (Carter et al., 1990). Our work suggests that ICEBERG, like IL-1ra, functions to keep IL-1β levels in check but does so by an intracellular desensitization mechanism. The essence of this involves the relatively slow protein synthesis–dependent accumulation of ICEBERG that negatively feeds back to inhibit binding of RIP2 to caspase-1 and also disrupts preformed RIP2/caspase-1 complexes. Hence, the temporal difference between the rapid, posttranslational RIP2 (or equivalent) mediated activation of caspase-1 and slow protein synthesis–dependent accumulation of the feedback inhibitor ICEBERG provides a window of opportunity for controlled generation of IL-1β so that its beneficial local proinflammatory effects predominate over potentially deleterious systemic effects. In a related manner, the induction of negative feedback inhibitors of inflammation such as ICEBERG may be the molecular mechanism that underlies the phenomenon of tolerance where, following multiple inflammatory stimuli, the cellular response is diminished (for reviews see Yoza et al., 1998; Zeisberger and Roth, 1998).

Components of the signaling pathway that mediate activation of RIP2 upon engagement of proinflammatory receptors such as the toll-like (TL) receptors remain unclear. Two adaptor molecules likely involved are MyD88 and TRAF6. Both have been shown to lie downstream of toll receptors and the IL-1 receptor (Medzhitov et al., 1998; Muzio et al., 1998b; Yang et al., 1999). Further-

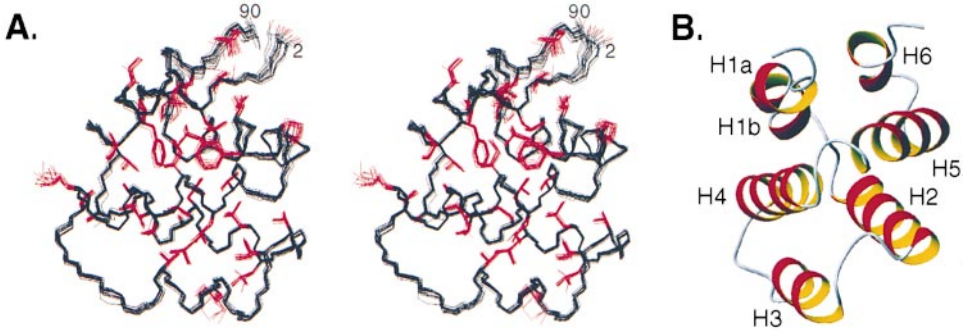

Figure 8. ICEBERG Structure

(A) Stereoview showing best fit superpositions (optimized for residues 5–89) of the backbone atoms (N, Cα, and C′) from the 20 NMR-derived structures of ICEBERG. The side chain heavy atoms of hydrophobic residues are shown in red. The RMSD with respect to the mean coordinates for this superposition is 0.25 ± 0.04 Å for the backbone atoms and 0.71 ± 0.05 Å for the heavy atoms.

(B) Schematic representation of the ICEBERG structure showing the packing of the six helices formed by residues 5–8 (H1a), 10–14 (H1b), 19–32 (H2), 37–44 (H3), 50–63 H4), 67–79 (H5), and 83–87 (H6). This figure was produced using the program MOLMOL (Koradi et al., 1996).

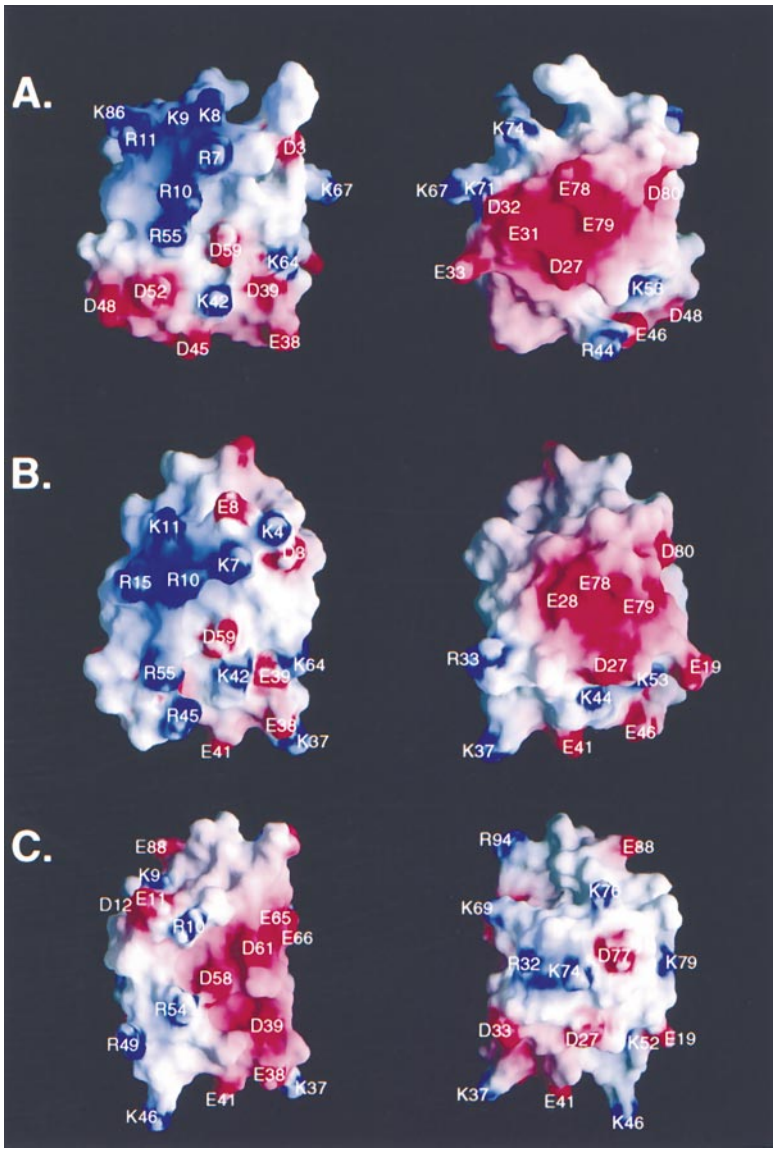

Figure 9. Surface Potentials of ICEBERG, Caspase-1, and RIP2

(A) The solvent-accessible molecular surface of the minimized mean structure of ICEBERG color coded according to electrostatic surface potential: red, −8 kT; white, 0 kT; and blue, +8 kT. The two views are related by a 180° rotation about the vertical axis.

(B) The electrostatic surface potential of the caspase-1 prodomain homology model.

(C) Electrostatic surface potential of the RIP2 CARD homology model. This figure was produced using the program GRASP (Nicholls, 1992).

more, mice homozygous null for MyD88 and TRAF6 are resistant to LPS challenge (Kawai et al., 1999; Lomaga et al., 1999). Significantly, TRAF6 has been shown to bind RIP2 (McCarthy et al., 1998) so that a possible scenario is for signaling information to flow from the receptor to MyD88 to TRAF6 and eventually to RIP2. This is conjecture at the moment and awaits experimental verification. RIP2 may be only one of many possible activators of caspase-1 and its precise contribution to this pathway will only be accurately gauged once RIP2 knockout mice are available.

Understanding the molecular basis of the interactions between the CARDs of ICEBERG, RIP2, and caspase-1 is central to understanding their role in modulating caspase-1 activation. To this end, we have determined the solution structure of ICEBERG and constructed homology models of the CARDs of caspase-1 and RIP2. The surface properties of ICEBERG and the caspase-1 prodomain are in general similar, with each having distinct positively and negatively charged surfaces (Figure 9). The CARDs of both RAIDD and Apaf-1 also have two highly polar surfaces on opposite sides of the domains, although the positions and sizes of these patches differ from those observed for ICEBERG, as well as from each other (Chou et al., 1998; Day et al., 1999; Qin et al., 1999; Vaughn et al., 1999; Zhou et al., 1999) (Figure 1A). The caspase-2 and -9 prodomains also have distributions of surface charge similar to their respective binding partners, RAIDD and Apaf-1 (Chou et al., 1998; Qin et al., 1999; Vaughn et al., 1999; Zhou et al., 1999). The acidic residues on H2 and H3 of Apaf-1 CARD have been shown to interact directly with basic residues on helices H1 and H4 of the caspase-9 prodomain (Qin et al., 1999; Zhou et al., 1999). Charge–charge interactions have also been proposed to mediate the homophilic CARD/CARD interaction between RAIDD and caspase-2 (Chou et al., 1998). As for the RAIDD/caspase-2 and Apaf-1/caspase-9 interactions, we propose that charge–charge interactions are important for mediating the ICEBERG/caspase-1 interaction. An important question is whether

an acidic patch on ICEBERG interacts with the basic patch on caspase-1 or vice versa.

Given that RIP2 CARD contains a prominent acidic patch, but no such basic patch, one might speculate that the convex, positively charged patch on caspase-1 prodomain (Figure 9B) binds the concave, negatively charged patch of RIP2 (Figure 9C). If this were true, and given that ICEBERG competes with RIP2 for caspase-1 binding, the basic patch on caspase-1 would also be predicted to bind an acidic patch on ICEBERG. However, preliminary mutagenesis experiments with ICEBERG suggest a more complicated model (unpublished data). Specifics of the interactions await detailed mutagenesis and structural analyses of the ICEBERG/caspase-1 prodomain and the RIP2 CARD/caspase-1 prodomain complexes.

Experimental Procedures

Plasmids, Transient Transfection Assays, Immunoprecipitation, and Western Blotting

cDNAs encoding gD-tagged caspase-1, HA-tagged ICEBERG, and Δprocaspase-1-FLAG (residues 103–404) were cloned into the mammalian expression vector pCDNA3. Expression constructs for FLAG-tagged wild-type and mutant caspase-1, -7, and -9 and for myc-his-tagged RIP2 have been described elsewhere (Duan et al., 1996a, 1996b; McCarthy et al., 1998; Thome et al., 1998).

For transient transfections, 293T cells were transfected using GenePorter (Gene Therapy Systems) according to the manufacturer's instructions. Cell lysis, immunoprecipitation analysis, and immunoblotting were performed as described previously (McCarthy et al., 1998) except for the addition of 3 mM DTT in the lysis buffer and the use of a light chain specific antibody (HRP-conjugated goat anti-mouse $F(ab)'_2$ – Jackson Labs) as the secondary reagent in Western blotting. Immunoprecipitation for endogenous caspase-1/RIP2 interaction was performed using 5×10^8 THP.1 cells grown in spinner flasks.

Monoclonal antibodies to caspase-1 prodomain, RIP2, and ICEBERG were made at Genentech using standard methods.

Metabolic Labeling

For ICEBERG expression and binding, 1×10^8 THP.1 cells or 2.5×10^6 primary monocytes were exposed to 100 ng/mL of LPS (List Biological Laboratories) for the indicated time and labeled with 500 μCi/mL of ^{35}S-cysteine and methionine (Translabel from ICN). For caspase-1 and RIP2 binding, the same number of cells were labeled as above for 30 min. Dialyzed fetal bovine serum tested for endotoxin was used (HyClone). Cell lysis and reimmunoprecipitation analysis were performed as described previously (O' Rourke et al., 1992).

ICEBERG Stable Cell Lines and Activation Assays

ICEBERG was cloned into the pCEP vector (Invitrogen) and stable clones made in 293T cells using standard molecular biology techniques. For in vivo activation studies, cells were transfected and lysed in activation buffer as descibed previously (Stennicke and Salvesen, 1997). For in vitro activation studies, in vitro translated caspase-1 was incubated in the presence of RIP2 with or without ICEBERG in a total volume of 40 μl of activation buffer overnight at 37°C.

Cytosolic extracts for determining caspase-1 activity were prepared as described previously (Yamin et al., 1996). Caspase-1 activity was measured in undialyzed lysate by the cleavage of the fluorescent peptide substrate Ac-WEHD-AMC as described previously (Thornberry et al., 1997).

Cell Lines, RNA Isolation, and RT-PCR

THP.1 acute monocytic cells (ATCC) and human umbilical vein endothelial cells (Clonetics) were cultured according to supplier's instructions. Primary monocytes were isolated from whole blood using Lymphocyte Separation Medium (ICN). RNA was isolated from cells solubilized with guanidine thiocyanate followed by cesium chloride gradient centrifugation. RT-PCR was performed according to instructions with the Perkin-Elmer RNA PCR kit using the oligo d(T) primer. Levels of RNA were normalized using human glyceraldehyde 3-phosphate dehydrogenase specific control primers (Clontech).

Northern Blot Analysis and cDNA Panel Analysis

Adult human multiple tissue Northern blots (Clontech) were hybridized according to manufacturer's instructions using radiolabeled full length ICEBERG. Levels of RNA were normalized to actin. Human adult cDNA panels (Clontech) were amplified using primers specific for ICEBERG, RIP2, or caspase-1. cDNA levels were normalized to human glyceraldehyde 3-phosphate dehydrogenase.

Retroviral Constructs, Transduction, and ELISA

ICEBERG was cloned into the MSCV hygromycin-selectable retroviral vector (Clontech) and recombinant virus obtained and titered following transfections of a 293 Phoenix packaging cell line (Kinsella and Nolan, 1996). Individual clones were assessed by immunoblotting for expression of ICEBERG. Control THP.1 cells or those expressing ICEBERG were stimulated with the indicated amount of LPS and release of mature IL-1β determined using the Quantikine ELISA kit (R&D Systems) according to the manufacturer's directions. At least two separate clones expressing ICEBERG were tested with similar results. Isolated primary monocytes were treated with 100 ng/mL of LPS, which was removed after 1 hr by extensive washing. The release of mature IL-1β was measured in the supernatant during the indicated time periods as above.

Protein Purification and Pure Protein Binding Assays

cDNAs encoding ICEBERG and the prodomain of caspase-1 (residues 1–92) were cloned into pET21a (Novagen) modified to contain *argU* (Garcia et al., 1986). The proteins were expressed from BL21(DE3) cells (Stratagene) and grown in a 2.5 L fermentation vessel (New Brunswick) in M9 minimal medium. For isotopic labeling, the M9 medium contained ^{15}N-NH_4Cl (2 g/L) and/or ^{13}C-glucose (2.5 g/L) (Martek). Cells were homogenized and lysed in the presence of 50 mM Tris (pH 8.0), 10mM DTT, 1mM EDTA, and protease inhibitors. The cell pellet was resuspended in phosphate buffered saline (PBS) and 50 mM $MgCl_2$ with 0.1 mg DNAase per 100 ml lysate. The mixture was stirred for 1 hr at room temperature and again centrifuged. The resulting pellet was resuspended in 7 M Gu-HCl, 50 mM NaH_2PO_4 (pH 5.0), 5 mM DTT, and 5 mM EDTA and loaded onto a Sephacryl S-100 (Pharmacia) sizing column. For ICEBERG, pooled protein fractions were diluted to 2 M Gu-HCl and refolded by dialysis with 50 mM NaH_2PO_4 (pH 5.0), 0.1 M NaCl, and 5mM DTT at a protein concentration of 0.18 mg/mL. The protein was dialyzed against 0.1% acetic acid and concentrated by lyophilization. The yield of purified protein was ~175 mg/L of cell culture.

For caspase-1 prodomain, the S-100 fractions were pooled and further purified on a C4 reverse phase HPLC column using a water/acetonitrile gradient in the presence of 0.1% trifluoroacetic acid. Caspase-1 prodomain fractions were next lyophilized and resuspended in the 7 M Gu-HCl solution as above. The protein was then diluted to 2 M Gu-HCl at a protein concentration of 0.1 mg/mL with 50 mM NaH_2PO_4 (pH 5.0), 0.1 M NaCl, 5 mM DTT, and 5 mM EDTA for refolding. Gu-HCl was removed by dialysis against the phosphate buffer. The protein solution was subsequently dialyzed into 0.1% acetic acid, and concentrated by lyophilization. The yield of purified protein was ~100 mg/L of cell culture. Electrospray mass spectrometry was used to verify the identity of the proteins; both purified ICEBERG and the prodomain caspase-1 were found to lack the N-terminal methionine residues.

ICEBERG was biotinylated with Sulfo-NHS-Biotin (Pierce). Binding assays were performed by incubating 4 μg of biotinylated ICEBERG with the caspase-1 prodomain at 4°C overnight in PBS. The volume was then brought up to 1 ml with 0.1% NP-40 lysis buffer followed by addition of monoclonal antibody to caspase-1 prodomain or 10 μl streptavidin beads (Sigma). Immune complexes were precipitated by the addition of Protein G beads (for caspase-1) or by streptavidin beads (for ICEBERG).

The CARD-containing segment of RIP2 (residues 454–540) was

cloned into the pGEX6P vector, expressed, and immobilized onto glutathione Sepharose beads. An excess of RIP2-glutathione Sepharose was incubated overnight with 4 μg of caspase-1 followed by addition of 4 μg of ICEBERG as a competitor. For the in vitro activation studies, caspase-1 was translated in the presence of ^{35}S-Methionine (Amersham) using the TNT T7 Quick coupled transcription/translation system (Promega). Five microliters of labeled caspase-1 was incubated with RIP2-glutathione Sepharose with or without 10 μg of ICEBERG.

Solution Structure

NMR spectra were acquired at 30°C on a Bruker DRX-500 spectrometer equipped with a 5 mm inverse ^{1}H/^{15}N/^{13}C-triple-resonance probe with three-axis gradient coils. Samples for NMR spectroscopy contained ~2 mM ICEBERG, 50 mM sodium acetate-d_3 (pH 3.8), 10–20 mM DTT-d_{10}, and 1.0 mM NaN_3. ^{1}H and ^{15}N resonance assignments were obtained using conventional NOESY-based methods (Wüthrich, 1986). The following spectra were recorded using a ^{15}N-labeled protein sample in 90% H_2O/10% D_2O: 2D 2QF-COSY, 2D ^{1}H-^{15}N HSQC, 3D TOCSY-HSQC (mixing times, 33 and 98 ms), 3D HNHA, 3D HNHB, 3D ^{15}N-NOESY-HSQC (mixing time, 100 ms), 3D ^{15}N-HMQC-NOESY-HMQC (mixing time, 100 ms), and 3D ^{15}N-ROESY-HSQC (mixing time, 40 ms) (Cavanagh et al., 1995). ^{13}C resonance assignments were completed using a uniformly ^{15}N/^{13}C-labeled protein sample in 90% H_2O/10% D_2O and the following experiments: 2D ^{1}H-^{13}C HSQC, 3D CBCA(CO)NH, 3D HCCH-TOCSY, and 3D ^{13}C-NOESY-HSQC (mixing time 100 ms) (Cavanagh et al., 1995). Stereospecific assignment of methyl groups of Val and Leu residues were obtained using a 15% ^{13}C-labeled sample (Neri et al., 1989). Distance and dihedral angle restraints were generated as described previously (Fairbrother et al., 1994, 1998). Structures of ICEBERG were calculated with a simulated annealing protocol using the program XPLOR 98.1 (Molecular Simulations, Inc.).

Structural Alignments and Modeling

Cα alignments with the CARDs of Apaf-1, caspase-9, and RAIDD were performed using the program ALIGN (Satow et al., 1986) and coordinates from the PDB (1CY5, 3YGS, and 3CRD). Structures of the prodomain of procaspase-1 and the CARD of RIP-2 were modeled using the Homology module of InsightII 98.0 (Molecular Simulations, Inc.).

Acknowledgments

We thank the Antibody Facility and Pathology Department at Genentech, Inc. for caspase-1, ICEBERG, and RIP2 antibodies; G. Pan for the original EST; T. Baker for the isolation of monocytes; J. Lee for library construction; J. Bourell for mass spectrometry; G. Solar for retroviral help; R. Garcia for biotinylating ICEBERG; and members of the Dixit lab, P. Carter, P. Polakis, A. Cochran, and N. Skelton for encouragement and discussions. E. W. H. is a fellow of the Medical Scientist Training Program and is supported by the MSTP NIH Training Grant T32 GM07863 and Genentech, Inc.

Received May 14, 2000; revised August 11, 2000.

References

Carter, D.B., Deibel, M.R., Jr., Dunn, C.J., Tomich, C.C.-S., Laborde, A.L., Slightom, J.L., Berger, A.E., Bienkowski, M.J., Sun, F.F., McEwan, R.N., et al. (1990). Purification, cloning, expression and biological characterization of an interleukin-1 receptor antagonist protein. Nature *344*, 633–638.

Cavanagh, J., Fairbrother, W.J., Palmer, A.G., III, and Skelton, N.J. (1995). Protein NMR Spectroscopy: Principles and Practice (San Diego: Academic Press).

Cerretti, D.P., Kozlosky, C.J., Mosley, B., Nelson, N., Ness, K.V., Greenstreet, T.A., March, C.J., Kronheim, S.R., Druck, T., Cannizzaro, L.A., et al. (1992). Molecular cloning of the interleukin-1β converting enzyme. Science *256*, 97–100.

Chou, J.J., Matsuo, H., Duan, H., and Wagner, G. (1998). Solution structure of the RAIDD CARD and model for CARD/CARD interaction in caspase-2 and caspase-9 recruitment. Cell *94*, 171–180.

Day, C.L., Dupont, C., Lackmann, M., Vaux, D.L., and Hinds, M.G. (1999). Solution structure and mutagenesis of the caspase recruitment domain (CARD) from Apaf-1. Cell Death Differ. *6*, 1125–1132.

Dinarello, C.A. (1997). Proinflammatory and anti-inflammatory cytokines as mediators in the pathogenesis of septic shock. Chest *112*, 321S–329S.

Duan, H., Chinnaiyan, A.M., Hudson, P.L., Wing, J.P., He, W.W., and Dixit, V.M. (1996a). ICE-LAP3, a novel mammalian homologue of the Caenorhabditis elegans cell death protein Ced-3 is activated during Fas- and tumor necrosis factor-induced apoptosis. J. Biol. Chem. *271*, 1621–1625.

Duan, H., Orth, K., Chinnaiyan, A., Poirier, G., Froelich, C.J., He, W.-W., and Dixit, V.M. (1996b). ICE-LAP6, a novel member of the ICE/Ced-3 gene family, is activated by the cytotoxic T cell protease Granzyme B. J. Biol. Chem. *271*, 16720–16724.

Eberstadt, M., Huang, B., Chen, Z., Meadows, R.P., Ng, S.C., Zheng, L., Lenardo, M.J., and Fesik, S.W. (1998). NMR structure and mutagenesis of the FADD (Mort1) death-effector domain. Nature *392*, 941–945.

Fairbrother, W.J., Reilly, D., Colby, T.J., Hesselgesser, J., and Horuk, R. (1994). The solution structure of melanoma growth stimulating activity. J. Mol. Biol. *242*, 252–270

Fairbrother, W.J., Champe, M.A., Christinger, H.W., Keyt, B.A., and Starovasnik, M.A. (1998). Solution structure of the heparin-binding domain of vascular endothelial growth factor. Structure *6*, 637–648.

Garcia, G.M., Mar, P.K., Mullin, D.A., Walker, J.R., and Prather, N.E. (1986). The E. coli dnaY gene encodes an arginine transfer RNA. Cell *45*, 453–459.

Ghayur, T., Banerjee, S., Hugunin, M., Butler, D., Herzog, L., Carter, A., Quintal, L., Sekut, L., Talanian, R., Paskind, M., et al. (1997). Caspase-1 processes IFN-gamma-inducing factor and regulates LPS-induced IFN-gamma production. Nature *386*, 619–623.

Gu, Y., Wu, J., Faucheu, C., Lalanne, J.L., Diu, A., Livingston, D.J., and Su, M.S. (1995). Interleukin-1 beta converting enzyme requires oligomerization for activity of processed forms in vivo. EMBO J. *14*, 1923–1931.

Gu, Y., Kuida, K., Tsutsui, H., Ku, G., Hsiao, K., Fleming, M.A., Hayashi, N., Higashino, K., Okamura, H., Nakanishi, K., et al. (1997). Activation of interferon-gamma inducing factor mediated by interleukin-1 beta converting enzyme. Science *275*, 206–209.

Hawley, R.G., Hawley, T.S., Fong, A.Z., Quinto, C., Collins, M., Leonard, J.P., and Goldman, S.J. (1996). Thrombopoietic potential and serial repopulating ability of murine hematopoietic stem cells constitutively expressing interleukin 11. Proc. Natl. Acad. Sci. USA *93*, 10297–10302.

Hofmann, K. (1999). The modular nature of apoptotic signaling proteins. Cell. Mol. Life Sci. *55*, 1113–1128.

Hofmann, K., Bucher, P., and Tschopp, J. (1997). The CARD domain: a new apoptotic signalling motif. Trends Biochem. Sci. *22*, 155–156.

Hu, S., Vincenz, C., Buller, M., and Dixit, V.M. (1997a). A novel family of viral death effector domain-containing molecules that inhibit both CD-95- and tumor necrosis factor receptor-1-induced apoptosis. J. Biol. Chem. *272*, 9621–9624.

Hu, S., Vincenz, C., Ni, J., Gentz, R., and Dixit, V.M. (1997b). I-FLICE, a novel inhibitor of tumor necrosis factor receptor-1- and CD-95-induced apoptosis. J. Biol. Chem. *272*, 17255–17257.

Huang, B., Eberstadt, M., Olejniczak, E.T., Meadows, R.P., and Fesik, S.W. (1996). NMR structure and mutagenesis of the Fas (APO-1/CD95) death domain. Nature *384*, 638–641.

Inohara, N., del Peso, L., Koseki, T., Chen, S., and Nunez, G. (1998). RICK, a novel protein kinase containing a caspase recruitment domain, interacts with CLARP and regulates CD95-mediated apoptosis. J. Biol. Chem. *273*, 12296–12300.

Irmler, M., Thome, M., Hahne, M., Schneider, P., Hofmann, K., Steiner, V., Bodmer, J.L., Schroter, M., Burns, K., Mattmann, C., et al. (1997). Inhibition of death receptor signals by cellular FLIP. Nature *388*, 190–195.

Jeong, E.J., Bang, S., Lee, T.H., Park, Y.I., Sim, W.S., and Kim, K.S. (1999). The solution structure of FADD death domain. Structural basis of death domain interactions of Fas and FADD. J. Biol. Chem. *274*, 16337–16342.

Kawai, T., Adachi, O., Ogawa, T., Takeda, K., and Akira, S. (1999). Unresponsiveness of MyD88-deficient mice to endotoxin. Immunity *11*, 115–122.

Kinsella, T.M., and Nolan, G.P. (1996). Episomal vectors rapidly and stably produce high-titer recombinant retrovirus. Hum. Gene Ther. *7*, 1405–1413.

Koradi, R., Billeter, M., and Wüthrich, K. (1996). MOLMOL: a program for display and analysis of macromolecular structures. J. Mol. Graph. *14*, 29–32.

Kuida, K., Lippke, J.A., Ku, G., Harding, M.W., Livingston, D.J., Su, M.S.-S., and Flavell, R.A. (1995). Altered cytokine export and apoptosis in mice deficient in interleukin-1β converting enzyme. Science *267*, 2000–2003.

Li, P., Allen, H., Banerjee, S., Franklin, S., Herzog, L., Johnston, C., McDowell, J., Paskind, M., Rodman, L., Salfeld, J., et al. (1995). Mice deficient in IL-1β-converting enzyme are defective in production of mature IL-1β and resistant to endotoxic shock. Cell *80*, 401–411.

Liepinsh, E., Ilag, L.L., Otting, G., and Ibáñez, C.F. (1997). NMR structure of the death domain of the p75 neurotrophin receptor. EMBO J. *16*, 4999–5005.

Linge, J.P., and Nilges, M. (1999). Influence of non-bonded parameters on the quality of NMR structures: a new force field for NMR structure calculations. J. Biomol. NMR *13*, 51–59.

Lomaga, M.A., Yeh, W.C., Sarosi, I., Duncan, G.S., Furlonger, C., Ho, A., Morony, S., Capparelli, C., Van, G., Kaufman, S., et al. (1999). TRAF6 deficiency results in osteopetrosis and defective interleukin-1, CD40, and LPS signaling. Genes Dev. *13*, 1015–1024.

MacCorkle, R.A., Freeman, K.W., and Spencer, D.M. (1998). Synthetic activation of caspases: artificial death switches. Proc. Natl. Acad. Sci. USA *95*, 3655–3660.

McCarthy, J.V., Ni, J., and Dixit, V.M. (1998). RIP2 is a novel NF-kappaB-activating and cell death-inducing kinase. J. Biol. Chem. *273*, 16968–16975.

Medzhitov, R., Preston-Hurlburt, P., Kopp, E., Stadlen, A., Chen, C., Ghosh, S., and Janeway, C.A., Jr. (1998). MyD88 is an adaptor protein in the hToll/IL-1 receptor family signaling pathways. Mol. Cell *2*, 253–258.

Miller, D.K., Ayala, J.M., Egger, L.A., Raju, S.M., Yamin, T.T., Ding, G.J., Gaffney, E.P., Howard, A.D., Palyha, O.C., Rolando, A.M., et al. (1993). Purification and characterization of active human interleukin-1β-converting enzyme from THP.1 monocyte cells. J. Biol. Chem. *268*, 18062–18069.

Muzio, M., Stockwell, B.R., Stennicke, H.R., Salvesen, G.S., and Dixit, V.M. (1998a). An induced proximity model for caspase-8 activation. J. Biol. Chem. *273*, 2926–2930.

Muzio, M., Natoli, G., Saccani, S., Levrero, M., and Mantovani, A. (1998b). The human toll signaling pathway: divergence of nuclear factor kappaB and JNK/SAPK activation upstream of tumor necrosis factor receptor-associated factor 6 (TRAF6). J. Exp. Med. *187*, 2097–2101.

Neri, D., Szyperski, T., Otting, G., Senn, H., and Wüthrich, K. (1989). Stereospecific nuclear magnetic resonance assignments of the methyl groups of valine and leucine in the DNA-binding domain of the 434 repressor by biosynthetically directed fractional ^{13}C labeling. Biochemistry *28*, 7510–7516.

Nicholls, A. (1992). GRASP: Graphical Representation and Analysis of Surface Properties, 1.2 Edition (New York: Columbia University).

O'Reilly, M., Newcomb, D.E., and Remick, D. (1999). Endotoxin, sepsis, and the primrose path. Shock *12*, 411–420.

O'Rourke, K.M., Laherty, C.D., and Dixit, V.M. (1992). Thrombospondin 1 and Thrombospondin 2 are expressed as both homo- and heterotrimers. J. Biol. Chem. *267*, 24921–24924.

Qin, H., Srinivasula, S.M., Wu, G., Fernandes-Alnemri, T., Alnemri, E.S., and Shi, Y. (1999). Structural basis of procaspase-9 recruitment by the apoptotic protease-activating factor 1. Nature *399*, 549–557.

Salvesen, G.S., and Dixit, V.M. (1999). Caspase activation: the induced-proximity model. Proc. Natl. Acad. Sci. USA *96*, 10964–10967.

Satow, Y., Cohen, G.H., Padlan, E.A., and Davies, D.R. (1986). Phosphocholine binding immunoglobulin Fab McPC603. An X-ray diffraction study at 2.7 Å. J. Mol. Biol. *190*, 593–604.

Srinivasula, S.M., Ahmad, M., Fernandes-Alnemri, T., and Alnemri, E.S. (1998). Autoactivation of procaspase-9 by Apaf-1-mediated oligomerization. Mol. Cell *1*, 949–957.

Stennicke, H.R., and Salvesen, G.S. (1997). Biochemical characteristics of caspases-3, -6, -7, and -8. J. Biol. Chem. *272*, 25719–25723.

Thome, M., Schneider, P., Hofmann, K., Fickenscher, H., Meinl, E., Neipel, F., Mattmann, C., Burns, K., Bodmer, J.L., Schroter, M., et al. (1997). Viral FLICE-inhibitory proteins (FLIPs) prevent apoptosis induced by death receptors. Nature *386*, 517–521.

Thome, M., Hofmann, K., Burns, K., Martinon, F., Bodmer, J.L., Mattmann, C., and Tschopp, J. (1998). Identification of CARDIAK, a RIP-like kinase that associates with caspase-1. Curr. Biol. *8*, 885–888.

Thornberry, N.A., Bull, H.G., Calaycay, J.R., Chapman, K.T., Howard, A.D., Kostura, M.J., Miller, D.K., Molineaux, S.M., Weidner, J.R., Aunins, J., et al. (1992). A novel heterodimeric cysteine protease is required for interleukin-1β processing in monocytes. Nature *356*, 768–774.

Thornberry, N.A., Rano, T.A., Peterson, E.P., Rasper, D.M., Timkey, T., Garcia-Calvo, M., Houtzager, V.M., Nordstrom, P.A., Roy, S., Vaillancourt, J.P., et al. (1997). A combinatorial approach defines specificities of members of the caspase family and Granzyme B. J. Biol. Chem. *272*, 17907–17911.

Tschopp, J., Irmler, M., and Thome, M. (1998a). Inhibition of fas death signals by FLIPs. Curr. Opin. Immunol. *10*, 552–558.

Tschopp, J., Thome, M., Hofmann, K., and Meinl, E. (1998b). The fight of viruses against apoptosis. Curr. Opin. Genet. Dev. *8*, 82–87.

Van Criekinge, W., Beyaert, R., Van de Craen, M., Vandenabeele, P., Schotte, P., De Valck, D., and Fiers, W. (1996). Functional characterization of the prodomain of interleukin-1β converting enzyme. J. Biol. Chem. *271*, 27245–27248.

Vaughn, D.E., Rodriguez, J., Lazebnik, Y., and Joshua-Tor, L. (1999). Crystal structure of Apaf-1 caspase recruitment domain: an α-helical greek key fold for apoptotic signaling. J. Mol. Biol. *293*, 439–447.

Walker, N.P.C., Talanian, R.V., Brady, K.D., Dang, L.C., Bump, N.J., Ferenz, C.R., Franklin, S., Ghayur, T., Hackett, M.C., Hammill, L.D., et al. (1994). Crystal structure of the cysteine protease interleukin-1β-converting enzyme: a $(p20/p10)_2$ homodimer. Cell *78*, 343–352.

Wilson, K.P., Black, J.-A.F., Thomson, J.A., Kim, E.E., Griffith, J.P., Navia, M.A., Murcko, M.A., Chambers, S.P., Aldape, R.A., Raybuck, S.A., and Livingston, D.J. (1994). Structure and mechanism of interleukin-1β converting enzyme. Nature *370*, 270–275.

Wüthrich, K. (1986). NMR of Proteins and Nucleic Acids (New York: John Wiley & Sons, Inc.).

Yamin, T.T., Ayala, J.M., and Miller, D.K. (1996). Activation of the native 45-kDa precursor form of interleukin-1-converting enzyme. J. Biol. Chem. *271*, 13273–13282.

Yang, X., Chang, H.Y., and Baltimore, D. (1998). Autoproteolytic activation of pro-caspases by oligomerization. Mol. Cell *1*, 319–325.

Yang, R.B., Mark, M.R., Gurney, A.L., and Godowski, P.J. (1999). Signaling events induced by lipopolysaccharide-activated toll-like receptor 2. J. Immunol. *163*, 639–643.

Yoza, B., LaRue, K., and McCall, C. (1998). Molecular mechanisms responsible for endotoxin tolerance. Prog. Clin. Biol. Res. *397*, 209–215.

Zeisberger, E., and Roth, J. (1998). Tolerance to pyrogens. Ann. NY Acad. Sci. *856*, 116–131.

Zhou, P., Chou, J., Olea, R.S., Yuan, J., and Wagner, G. (1999). Solution structure of Apaf-1 CARD and its interaction with caspase-9 CARD: a structural basis for specific adaptor/caspase interaction. Proc. Natl. Acad. Sci. USA *96*, 11265–11270.

Zou, H., Henzel, W.J., Lui, X., Lutschg, A., and Wang, X. (1997). Apaf-1, a human protein homologous to *C. elegans* CED-4, participates in cytochrome c-dependent activation of caspase-3. Cell *90*, 405–413.

Zou, H., Li, Y., Liu, X., and Wang, X. (1999). An APAF-1 cytochrome c multimeric complex is a functional apoptosome that activates procaspase-9. J. Biol. Chem. *274*, 11549–11556.

GenBank Accession Numbers and Protein Data Bank ID Codes

The full sequence of ICEBERG has been deposited into GenBank with the accession number AF208005. The coordinates of the final 20 structures have been deposited into the Protein Data Bank with the accession code 1DGN.